Оптический журнал

Физическая оптика

Plasmonic circular dichroism of tailed spatial cross-shaped nanostructure

© 2018 Fei Wang, Tong Fu, Yongkai Wang, Yu Zhang, Zhongyue Zhang, Li Wang

School of Physics and Information Technology, Shaanxi Normal University, Xi'an 710119, China

E-mail: l.wang@snnu.edu.cn

Submitted 09.06.2017

Artificial chiral plasmonic nanostructure with strong circular dichroism (CD) has wide applications in biological monitoring, analytic chemistry, and optical property researching. In this paper, a tail is introduced to break the symmetry of metal spatial cross-shaped nanostructure to create chiral property. Finite element method calculating results show that dipole of upper tailed nanorod and that of bottom nanorod form Born–Kuhn model. CD effect depends strongly on the length and the orientation of introduced nanorod. This work provides novel way to generate tunable CD effect and provides potential application for further optimization.

Keywords: *circular dichroism, plasmon, electric dipole, Born–Kuhn model.*

OCIS codes: *240.5420, 240.6680, 260.3910.*

Циркулярный плазмонный дихроизм в крестовидных наноструктурах с хвостом в виде наностержня

© 2018 Fei Wang, Tong Fu, Yongkai Wang, Yu Zhang, Zhongyue Zhang Li Wang*

Искусственные хиральные плазмонные наноструктуры с выраженным циркулярным дихроизмом широко применяются в биологическом мониторинге, аналитической химии и исследовании оптических свойств материалов. В настоящей работе для придания хиральных свойств металлическим крестообразным наноструктурам к последним присоединялся хвост. Вычисления методом конечных разностей показали, что диполи с верхним и нижним закреплением хвоста-наностержня соответствуют модели Борна–Куна. Эффект вращения плоскости поляризации сильно зависит от размеров и ориентации присоединенного наностержня. Результаты данной работы открывают новые пути для получения управляемого эффекта циркулярного дихроизма с возможностями дальнейшей оптимизации.

Ключевые слова: *циркулярный дихроизм, плазмон, электрический диполь, модель Борна–Куна.*

INTRODUCTION

Chiral structure cannot be made to coincide with its mirror image. Chiral structure and its image are called chiral enantiomer [1–5]. Circular dichroism (CD), defined by the distinction of transmittance between left-handed circular polarized (LCP) and right-handed circular polarized (RCP) light, is widely-used spectroscopic technique to detect chirality property and study the conformation of structure [6, 7]. Most natural CD is intrinsic weak. Chiral plasmonic nanostructure shows stronger CD because of surface plasmon resonance, which possesses wide applications in biological monitoring [8, 9], analytic chemistry [10], and negative refractive index media [11].

There are many researches and widely-using methods introduced about the induction of CD effect. Either chiral structures or oblique incident direction can create asymmetric property. For instance, the sample of natural chiral structure leads to the CD signal, such as spiral and helix [12, 13]. Another typically type of chiral structure is bilayer twisted

nanostructures, where there magnetic and electric resonances arise at the same time, which have giant CD [14, 15]. Furthermore, plane chiral asymmetric structures, such as swastika [16, 17], asymmetric slit [18] and other chiral structures that have perceived vision of "twist" [19]. Compared with chiral structure, using the oblique incident beam [20, 21] to illuminate the symmetric sample is another method to create asymmetry and produce CD effect.

In this paper, one nanorod is adhered to the tail of original spatial cross-shaped nanostructure (SCN), which is achiral, to break the symmetry of SCN and generate CD effect. The effects of the length and the orientation of tail on CD signals of tailed spatial cross-shaped nanostructure (TSCN) are also studied. This study not only provides novel way to generate tunable CD effect but also provide potential applications in detection field based on CD signals.

STRUCTURE AND COMPUTATIONAL METHOD

The schematic of gold TSCN array is shown in fig. 1a. The TSCN array rests in the air environment. Figure 1b shows the orientation of tail with respect to upper nanorod and the illustration of geometric parameters. The lengths, widths, and heights of upper and bottom nanorods are denoted as $l_1 = l_2 = 100$ nm, $w_1 = w_2 = 20$ nm, and $h_1 = h_2 = 20$ nm. The separation between upper and bottom nanorod is fixed at 30 nm. The additional tail has the same cross section as those of two perpendicular nanorods. Spherical coordinate system is used to describe the orientation of tail. Radial distance r is defined by the effective distance as the tail start to rotating. Azimuth angle φ at xy plane and polar angle θ at xz plane are defined. The tail of TSCN is showed in fig. 1a with $r = 50$ nm, $\varphi = 0°$ and $\theta = 90°$.

The transmission properties of TSCN array were numerically simulated by the finite element method software of COMSOL Multiphysics. The excitation sources of incident beam are RCP light and LCP light traveling along the z-direction. The refractive index of Au is taken from Ref. [22]. In this study, the periods of the TSCN array are both fixed at 200 nm in the x and y directions. T is transmittance of incident polarized light, which is defined by the rate of output power P_{out} to input power P_{in}. The polarized states of RCP light and LCP light are represented as + and −. T_{++} (T_{--}) means that RCP (LCP) light simulating and receiving. The circular dichroism of circularly polarized light is defined as $CD = T_{++} - T_{--}$.

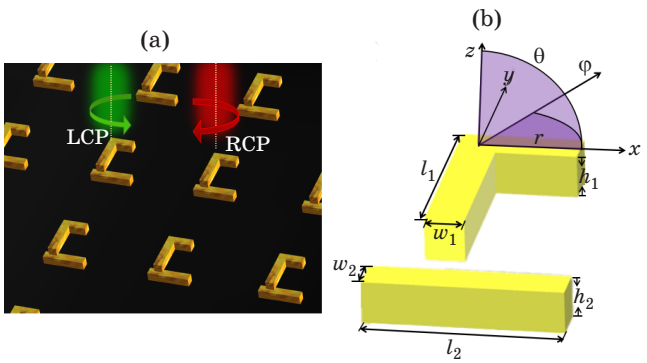

Fig. 1. (a) Schematic diagram of gold TSCN array with $r = 50$ nm, $\varphi = 0°$ and $\theta = 90°$ and (b) the position of spherical coordinate and the illustration of geometric parameters.

RESULTS AND DISCUSSION

Figure 2a shows the circular polarized transmittance spectra of TSCN with $r = 50$ nm, $\varphi = 0°$, and $\theta = 90°$ under RCP and LCP light illuminations. Four obvious resonant valleys appear at around 900, 770, 620 and 470 nm, respectively. For simplicity, these modes are marked as modes I, II, III and IV. Figure 2b shows the CD spectrum of TSCN (blue line added solid circle symbols) with $r = 50$ nm, $\varphi = 0°$, and $\theta = 90°$. It can be clearly observed that strong CD signals occur around resonant wavelengths.

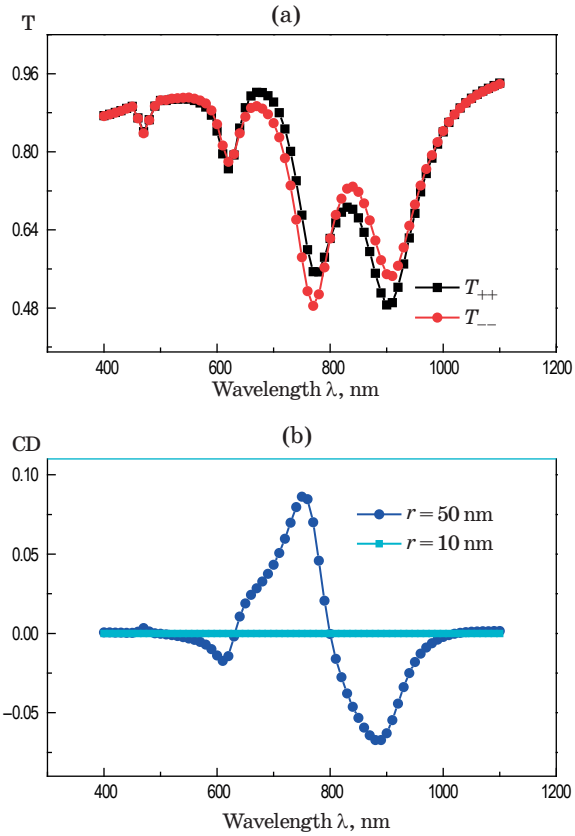

Fig. 2. (a) RCP light and LCP light transmittance spectra of TSCN with $r = 50$ nm, $\varphi = 0°$ and $\theta = 90°$, and (b) circular dichroism (CD) spectra of TSCN (blue line added solid circle symbols) with $r = 50$ nm, $\varphi = 0°$ and $\theta = 90°$ and SCN (cyan line added solid square symbols) with $r = 10$ nm, $\varphi = 0°$ and $\theta = 90°$.

The CD spectrum of SCN (cyan line added solid square symbols) with $r = 10$ nm, $\varphi = 0°$, and $\theta = 90°$ is also plotted in fig. 2b. Due to the symmetry of SCN, there is no CD signal appeared. The tail of upper nanorod breaks the symmetry of SCN and strong CD effect generated for TSCN.

To study the mechanism of these modes, the distributions of surface electric charge density of TSCN at corresponding resonant modes are calculated, as shown in fig. 3. The dipole of upper nanorod and dipole of tail are marked by the pink arrow, and the vector sum of upper dipoles is marked by the pink dash arrow. The dipole of bottom nanorod is marked by the blue arrow. At $\lambda_I = 900$ nm (mode I), a great number of positive charges distribute at the tail shown in fig. 3a, which forms a tilt strong dipole P_{IU} of upper nanorod, the equivalent dipole is depicted in fig. 3b. On the contrary, skimp charge appears at bottom nanorod, which forms a weak dipole P_{IB}. Dipoles at upper tailed nanorod and bottom nanorod form a bonding mode. At $\lambda_{II} = 770$ nm (mode II), minor charges appear at upper tailed nanorod as shown in fig. 3c. Positive charges mainly distribute at one part of the end of upper nanorod, and negative charges distribute at the tail but coming close to upper nanorod, which forms a weak tilt dipole P_{IIU}. The electric oscillation length of P_{IIU} is shorter than P_{IU}, as a result, mode II occurs at shorter wavelength. For bottom nanorod, large charges appear at the end of bottom nanorod and a strong dipole P_{IIB} is formed. P_{IIU} and P_{IIB} form a bonding mode as shown in fig. 3d. The electron oscillation of Mode I mainly distribute at the upper tailed nanorod, and that of Mode II mainly distribute at the bottom nanorod. At $\lambda_{III} = 620$ nm (mode III), negative charges appear at two ends of the tailed nanorod and positive charges appear at its middle part shown in fig. 3e, and these crossing dipoles of tailed nanorod composed a tilted dipole P_{IIIU}. And positive charges appear at the end of bottom nanorod, which form a dipole P_{IIIB}. Dipoles P_{IIIU} and P_{IIIB} form an anti-bonding mode as given in fig. 3f. The resonant wavelength of Mode III creates due to the electron oscillation on the tailed nanorod. As shown in fig. 3g and fig. 3h, negative charges appear at two ends of the tailed nanorod and positive charges appear at its middle part so that the crossing dipoles at upper tailed nanorod compose a weak tilted dipole P_{IVU} at $\lambda_{IV} = 470$ nm (mode IV). Large charges appear at the end of bottom nanorod, which forms a strong dipole P_{IVB}. The dipole P_{IVB} tilts to comes close to y-axial and the oscillating length decreases so that the magnitude of P_{IVB} is less than P_{IIIB}. This is the reason why mode IV occurs at shorter wavelength than mode III. Mode IV is an anti-bonding mode formed by composed dipole of tailed nanorod P_{IVU} and P_{IVB}. The oscillating intensity at $\lambda_{IV} = 470$ nm is weak than that at $\lambda_{III} = 620$ nm, so the CD magnitude of mode IV is tiny. This investigation corresponds to the regulation that anti-bonding mode occurs at shorter wavelength, and the bonding mode occurs at longer wavelength. Figure 3 shows the analytic modes by using the Born–Kuhn model [23] and explained by plasmonic coupling mechanism [24–29]. The original electric dipoles of upper nanorod and bottom nanorod are perpendicular special crossing. However, when tailed nanorod is added, the electric dipoles of upper tailed nanorod and bottom nanorod are tilted crossing. Tilt of the composed dipole leads to asymmetric property of composed structure and the induction of CD effect. These kinds of resonant mode with the positions of different wavelengths are distinct and lead to different CD effects.

Figure 4 shows the CD spectra of TSCN at $\varphi = 0°$ and $\theta = 90°$ with different r. There are four modes appeared in the spectra. When r increased by step

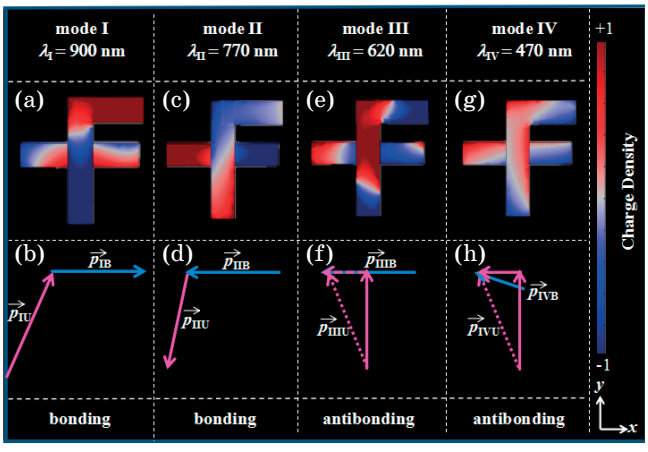

Fig. 3. (a), (c), (e) and (g) show that the surface charge distributions of mode I, mode II, mode III and mode IV in RCP spectra, and (b), (d), (f) and (h) show that the illustration of dipole at each corresponding resonant wavelength.

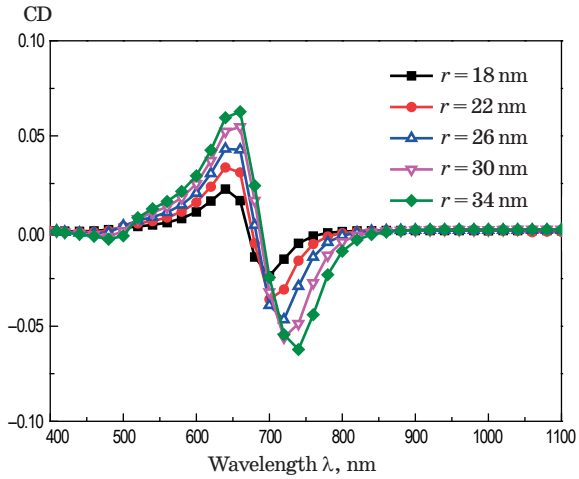

Fig. 4. Circular dichroism (CD) spectra of TSCN with different r increased by step of 4 nm from 18 nm to 34 nm at $\varphi = 0°$ and $\theta = 90°$.

of 4 nm from 18 nm to 34 nm, the magnitudes of CD effects at four modes increased and the resonance wavelength of mode I shifts from 700 nm to 740 nm stepped by 10 nm. The tail can make the composed dipole of upper tailed nanorod tilted. The longer the tail is, the smaller tilted angle of two spatial-crossing dipole modes will be. The tilt angle can influence the effective length of dipole of upper tailed nanorod to lead to red or blue shift of resonant wavelength. So r can influence the resonant wavelength of mode I that the resonant wavelength red shifts as r increasing. The longer electron oscillation length of mode I leads to longer interacting distance of P_{IU}, hence red shift occurs.

To investigate effect of the orientation of tail, the CD spectra of TSCN by changing azimuth angle φ with fixed parameters of r = 50 nm and θ = 90° is showed in fig. 5. The changing of φ influences the magnitude of CD effect. As φ changing by step of 30° from 0° to 180°, the resonant wavelengths keep constant except for the resonant wavelength of mode I. As φ increasing at the range of 0° to 90°, the resonant wavelength of mode I shifts from 890 nm to short position, and magnitude of CD signal gradually decreases from about 0.087 to zero by adding angle size. As φ increasing at the range of 90° to 180°, the resonant wavelength of mode I red shifted to 890 nm, and the magnitude of CD signal gradually is also increased from zero to about 0.087. The CD signal is approach to zero as the magnitude of φ is 90° due to the symmetric composed structure like SCN. From fig. 5, it obviously shows these CD signal curves at ranges of 0° to 90° and 90° to 180° are symmetric about CD = 0 line. As φ changing from 90° to 180°, the situation is opposite with that of 0° to 90°. Comparing with the situation at 180° − φ, symbol of CD signal at angle φ is opposite, and the magnitude of CD signal at angle φ is same

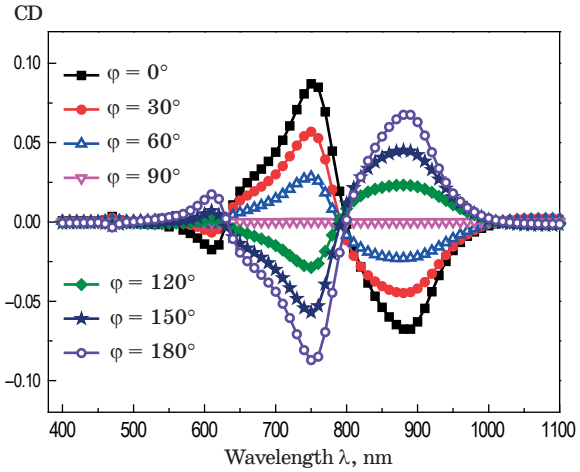

Fig. 5. Circular dichroism (CD) spectra of TSCN with different φ increased by step of 30° from 0° to 180° at r = 50 nm and θ = 90°.

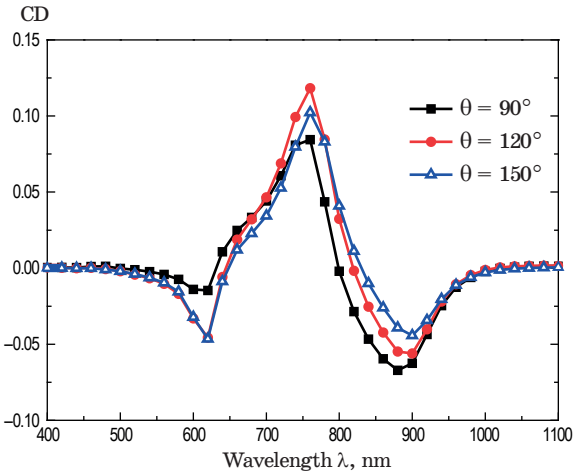

Fig. 6. Circular dichroism (CD) spectra of TSCN with different θ increased by step of 30° from 90° to 150° at r = 50 nm and φ = 0°.

as the condition of 180° − φ. This effect is same as the situation of chiral molecule and its enantiomer. The angle φ changes the tilt degree of composed dipole and changes the interacting distance of upper composed dipole so that the resonant wavelength blue shifts or red shifts at mode I. It is satisfied the explained mechanism about BK model.

The CD spectra of TSCN with different polar angle θ and fixed parameters of r = 50 nm and φ = 0° is calculated to gain further insight of CD mechanism. It can be clearly identified in fig. 6 that the changing of θ can also influence CD effect. As θ increasing at step of 30° from 90° to 150°, the wavelengths of modes I and II both shift to longer positions. The wavelengths of modes I shift from 870 nm to 900 nm. This is due to the distance between tailed nanorod and bottom nanorod increases as θ increasing. The coupling between tailed nanorod and bottom nanorod enhances with more charges coming close to the end of tail and the interacting distance lengthening. So the wavelengths of mode I and mode II shift to longer position as θ increasing.

CONCLUSIONS

A tail has been utilized to break the symmetry of spatial cross-shaped nanostructure and induce remarkable CD effect. Simulation results indicate that the CD effect is strongly depending upon the length and the rotating angles of tail. Mechanism based on chiral plasmonic Born–Kuhn model has utilized to explain the CD effect. With the advantage of tail controlled sign and magnitude of CD signal potential applications such as chiral sensing may be achieved. This study provides a convenient method for further optimization and tuning of plasmonic chirality.

This work was supported by National Nature science Foundation of China (NSFC) (61575117), National college students Innovation-Training Project Foundation of China (201610718012), Fundamental Research Funds for the Central Universities of Ministry of Education of China (GK201603015), and Excellent PhD Dissertation Foundation of Shaanxi Normal University (X2014YB08).

REFERENCES

1. *Barron L.D., Long D.A.* Molecular light scattering and optical activity // J. Raman Spectrosc. 1983. V. 14. № 14. P. 219–219.
2. *Govorov A.O., Fan Z.Y., Pedro H., Slocik J.M., Naik R.R.* Theory of circular dichroism of nanomaterials comprising chiral molecules and nanocrystals: plasmon enhancement, dipole interactions, and dielectric effects // Nano Lett. 2010. V. 10. № 4. P. 1374–1382
3. *Nadia A.A., Fan Z., Tonooka T., Sharon M.K., Nikolaj G., Euan H., Alexander O.G., Malcolm K.* Induced chirality through electromagnetic coupling between chiral molecular layers and plasmonic nanostructures // Nano Lett. 2012. V. 12. № 2. P. 977–983.
4. *Xia Y.S., Zhou Y.L., Tang Z.Y.* Chiral inorganic nanoparticles: origin, optical properties and bioapplications // Nanosale. 2011. V. 3. № 4. P. 1374–1382.
5. *Zhao R., Zhang L., Zhou J., Koschny T., Soukoulis C.M.* Conjugated gammadion chiral metamaterial with uniaxal optical activity and negative refractive index // Phys. Rev. B 2011. V. 83. № 3. P. 035–105.
6. *Hendry E., Carpy T., Johnston J., Popland M., Mikhaylovskiy R.V., Lapthorn A.J., Kelly S.M., Barron L.D., Gadegaard N., Kadodwala M.* Ultrasensitive detection and characterization of biomolecules using superchiral fields // Nature Nanotech. 2010. V. 5. № 11. P. 783–787.
7. *Ernst K.H.* Molecular chirality at surfaces // Phys. Status Solidi. 2012. V. 249. № 11. P. 2057–2088.
8. *Robert W.J.* Bioinformatics analyses of circular dichroism protein reference databases // Bioinformatics. 2005. V. 21. № 23. P. 4230–4238.
9. *Kelly S.M., Jess T.J., Price N.C.* How to study proteins by circular dichroism // Biochimi. Biophys. Acta – Proteins & Proteomics. 2005. V. 1751. № 2. P. 119–139.
10. *Zhu Y., Xu L., Ma W., Xu Z., Kuang H., Wang L., Xu C.* A one-step homogeneous plasmonic circular dichroism detection of aqueous mercury ions using nucleic acid functionalized gold nanorods // Chem. Commun. 2012. V. 48. P. 11889–11891.
11. *George V.E., Ashwin K.I., Peter C.K.* Planar negative refractive index media using periodically L-C loaded transmission lines // IEEE. 2002. V. 50. № 12. P. 2702–2712.
12. *Ben M.M., Yulia C., Alexander B.T., Omri B.E., Fan Z.Y., Alexander O.G., Gil M.* Amplification of chiroptical activity of chiral biomolecules by surface plasmons // Nano Lett. 2014. V. 13. № 3. P. 1203–1209.
13. *Gansel J.K., Thiel M., Rill M.S., Decker M., Bade K., Saile V., Freymann G.V., Linden S., Wegener M.* Gold helix photonic metamaterial as broadband circular polarizer // Science. 2009. V. 325. № 5947. P. 1513–1515.
14. *Xiong X., Sun W.H., Bao Y.J., Peng R.W., Wang M., Sun C., Lu X., Shao J., Li Z.F., Ming N.B.* Switching the electric and magnetic responses in a metamaterial [J] // Phys. Rev. B. 2009. V. 80. № 20. P. 2665–2668.
15. *Tang Y., Sun L., Cohen A.E.* Chiroptical hot spots in twisted nanowire plasmonic oscillators [J] // Appl. Phys. Lett. 2013. V. 102. № 4. P. 043–103.
16. *Kwon D.H., Werner P.L., Werner D.H.* Optical planar chiral metamaterial designs for strong circular dichroism and polarization rotation // Opt. Express. 2008. V. 16. № 16. P. 11802–11807.
17. *Cao T., Zhang L., Simpson R.E., Wei C.W., Cryan M.J., Cao T.* Strongly tunable circular dichroism in gammadion chiral phase-change metamaterials // Opt. Express. 2008. V. 21. № 23. P. 27841–27851.
18. *Nasimuddin, Qing X.M., Chen Z.N.* Compact asymmetric-slit microstrip antennas for circular polarization // IEEE T. Antenn. Propag. 2011. V. 59. № 1. P. 285–288.
19. *Schwanecke A.S., Krasavin A., Bagnall D.M., Potts A.Z., Zheludev A.V., Zheludev N.I.* Broken time reversal of light interaction with planar chiral nanostructures // Phys. Rev. Lett. 2003. V. 91. № 24. P. 247404.
20. *Lee S., Wang Z.B., Cheng F., Jiao J., Khan A., Li L.* Circular dichroism in planar extrinsic chirality metamaterial at oblique incident beam // Opt. Commun. 2013. V. 309. № 7. P. 201–204.
21. *Tian X.R., Fang Y.R., Zhang B.L.* Multipolar fano resonances and fano-assisted optical activity in silver nanorice heterodimers // ACS Photonics. 2014. V. 1. № 11. P. 1156–1164.
22. *Johnson P.B., Christy R.W.* Optical constants of the noble metals // Phys. Rev. B. 1972. V. 6. № 12. P. 4370–4379.

23. *Yin X., Schaferling M., Metzger B., Giessen H.* Interpreting chiral nanophotonic spectra: the plasmonic Born–Kuhn model // Nano Lett. 2013. V. 13. № 12. P. 6238–6243.

24. *Lu X.X., Wu J., Zhu Q.N., Zhao J.W., Wang Q.B., Zhan L., Ni W.H.* Circular dichroism from single plasmonic nanostructures with extrinsic chirality // Nanoscale. 2014. V. 6. № 23. P. 14244–14253.

25. *Wang Y.K., Qin Y., Zhang Z.Y.* Extraordinary optical transmission property of x-shaped plasmonic nanohole arrays // Plasmonics. 2014. V. 9. P. 203–207.

26. *Gansel J. K., Latzel M., Frolich A., Kaschke J., Thiel M., Wegener M.* Tapered gold-helix metamaterials as improved circular polarizers 100(10) // Appl. Phys. Lett. 2012. V. 100. № 10. P. 101109.

27. *Martin S., Daniel D., Mario H., Harald G.* Tailoring enhanced optical chirality: design principles for chiral plasmonic nanostructures // Phys. Rev. X. 2012. V. 2. № 3. P. 4186–4190.

28. *Teperik T.V., De Abajo F.G., Borisov A.G., Abdelsalam M., Bartlett P.N., Sugawara Y., Baumberg J.J.* Omnidirectional absorption in nanostructured metal surfaces // Nature photon. 2008. V. 2. № 5. P. 299–301.

29. *Vidal X., Kim W.J., Baev A., Tokar V., Jee H.,* Swihart *M.T., Prasad N.P.* Coupled plasmons induce broadband circular dichroism in patternable films of silver nanoparticles with chiral ligands // Nanoscale. 2013. V. 5. № 21. P. 10550–10555.